Title

The Mus81-Mms4 structure-selective endonuclease requires nicked DNA junctions to undergo conformational changes and bend its DNA substrates for cleavage

Journal

Nucleic Acids Research, 42(10)

ISSN

0305-1048

Authors

Mukherjee, Sucheta
Wright, William Douglass
Ehmsen, Kirk Tevebaugh
et al.

Publication Date

2014-06-02

DOI

10.1093/nar/gku265

Peer reviewed

Published online 17 April 2014 *Nucleic Acids Research, 2014, Vol. 42, No. 10* ***6511–6522***
doi: 10.1093/nar/gku265

The Mus81-Mms4 structure-selective endonuclease requires nicked DNA junctions to undergo conformational changes and bend its DNA substrates for cleavage

Sucheta Mukherjee[1,†], William Douglass Wright[1,†], Kirk Tevebaugh Ehmsen[1,†] and Wolf-Dietrich Heyer[1,2,*]

[1]Department of Microbiology & Molecular Genetics, University of California, One Shields Ave., Davis, Davis CA 95616–8665, USA and [2]Department of Molecular & Cellular Biology, University of California, One Shields Ave., Davis, Davis CA 95616–8665, USA

Received August 1, 2013; Revised March 18, 2014; Accepted March 19, 2014

ABSTRACT

Mus81-Mms4/EME1 is a DNA structure-selective endonuclease that cleaves joint DNA molecules that form during homologous recombination in mitotic and meiotic cells. Here, we demonstrate by kinetic analysis using physically tethered DNA substrates that budding yeast Mus81-Mms4 requires inherent rotational flexibility in DNA junctions for optimal catalysis. Förster Resonance Energy Transfer experiments further reveal that recognition of 3′-flap and nicked Holliday junction substrates by Mus81-Mms4 involves induction of a sharp bend with a 100° angle between two duplex DNA arms. In addition, thiol crosslinking of Mus81-Mms4 bound to DNA junctions demonstrates that the heterodimer undergoes a conformational change induced by joint DNA molecules with preferred structural properties. The results from all three approaches suggest a model for catalysis by Mus81-Mms4 in which initial DNA binding is based on minimal structural requirements followed by a rate-limiting conformational transition of the substrate and protein. This leads to a sharply kinked DNA molecule that may fray the DNA four base pairs away from the junction point to position the nuclease for cleavage between the fourth and fifth nucleotide. These data suggest that mutually compatible conformational changes of Mus81-Mms4 and its substrates tailor its incision activity to nicked junction molecules.

INTRODUCTION

Mus81-Mms4/EME1 is a heterodimeric endonuclease at the interface of DNA replication and homologous recombination (HR). When replication forks (RF) encounter DNA damage, they rely on HR to reference intact homologous sequence information at another locus. In this process, joint DNA molecules form between damaged and undamaged chromatids. These joint molecules can be processed by endonucleolytic strand incision(s) for replication to continue. An understanding of the nature of the DNA intermediates in these pathways and the types of joint molecules that Mus81-Mms4 cleaves *in vivo* is still developing.

In the budding yeast *Sacharomyces cerevisiae*, *mus81* or *mms4* deletion mutants are hypersensitive to any type of genotoxic agent that either blocks or stalls DNA replication (1,2) including hydroxurea (HU), methyl methansulfonate (MMS), camptothecin (CPT) or ultraviolet light. Mammalian cells lacking or depleted of MUS81-EME1 are hypersensitive to DNA interstrand crosslinking (ICL) agents, yet not to the entire spectrum of replication inhibitors as the yeast mutant (3). This could either mean that MUS81-EME1 does not respond to the types of damage or that other factors/pathways can substitute for MUS81-EME1 in mammals. Supporting the latter possibility, HU leads to MUS81-EME1-dependent double-strand DNA breaks (DSBs) in mammalian cells, yet $MUS81^{-/-}$ cells do not show overt hypersensitivity to HU (4).

Multiple lines of evidence support the view that Mus81-Mms4 incises DNA joint molecules that are generated by HR. First, Mus81 was initially identified as an interacting partner of the central HR protein Rad54 (2). The biological significance of this interaction is further supported by the

*To whom correspondence should be addressed. Tel: +1 530 752 3001; Fax: +1 530 752 3011; Email: wdheyer@ucdavis.edu
†The authors wish it to be known that, in their opinion, the first three authors should be regarded as Joint First Authors.
Present address:
Kirk Tevebaugh Ehmsen, Department of Cellular & Molecular Pharmacology, University of California, San Francisco, San Francisco, CA 94158, USA.

biochemical stimulation of Mus81-Mms4/EME1 nuclease activity by Rad54 (5,6). Second, the synthetic lethality between mutations in *MUS81* and *MMS4* in conjunction with defects in the Sgs1-Top3-Rmi1 complex is suppressed by HR defects that compromise Rad51 filament and displacement loop (D-loop) formation (*rad51, rad52, rad54, rad55, rad57*). The Sgs1-Top3-Rmi1 complex has been implicated in several steps of HR, including end resection, dissolution of joint molecules such as D-loops or double Holliday junctions (HJs), and branch migration. The complex also plays a role in checkpoint signaling and replication termination (7). The recombination-dependent synthetic lethality strongly suggests that Mus81-Mms4 acts in an alternate pathway to Sgs1-Top3-Rmi1 in the processing of HR-mediated joint molecules (8–10. Third, Rad51 foci, an *in vivo* mark of eukaryotic DNA strand exchange protein filaments on single-stranded (ssDNA) or heteroduplex DNA (hDNA), form in mouse embryonic fibroblasts (MEFs) treated with the DNA ICL agent mitomycin C (MMC), but persist in the absence of Mus81-Mms4 (3). This suggests that Mus81-Mms4 acts after Rad51 filament assembly and function. This conclusion is further corroborated by genetic analysis showing a role of Mus81-Mms4 in mitotic and meiotic crossover formation (11,12). Accordingly, Mus81-Mms4 contributes to HR-mediated RF support by targeting recombination intermediates that form downstream of HR initiated on newly exposed ssDNA at stalled or collapsed forks.

There is also evidence that Mus81-Mms4/EME1 may function upstream of HR, possibly by cleaving unprotected RFs to initiate HR. Detailed genetic analysis in budding yeast identified Rad51- (hence HR-) independent functions of Mus81 (13). Moreover, Hanada *et al.* (4) described the Mus81-Mms4-dependent formation of DSBs in response to replication inhibition in MEFs. They assessed DSBs by resolving intact chromosomes from chromosome fragments using pulsed-field electrophoresis. In wild type MEFs cells, but not *MUS81*$^{-/-}$ cells, these broken chromosomes (presumably one-sided DSBs), form 18–24 h after the replication block. It was later shown that chemical DNA damage was not necessary for Mus81-Mms4-dependent DSB formation, but that stalling the DNA polymerase with HU or aphidicolin also led to DSB formation with similar kinetics as for MMC (14). Two other studies demonstrated Mus81-dependent break formation in response to HU or aphidicolin in fission yeast (15) and mammalian cells (16). However, unlike the Hanada studies (4,14), formation of these DSBs required inactivation of Cds1/Chk2. The breaks also formed much faster than 18 h—within hours in fission yeast and minutes in human cells. These differences in the kinetics of break formation can be explained by stabilization of stalled forks by DNA damage checkpoints (17), which is overcome either by disabling the checkpoints or by prolonged stall time (18). Similar fork cleavage by MUS81-EME1 was demonstrated in mammalian cells when fork stalling was induced by Topoisomerase I-DNA complexes (19).

Recent studies (20–23) have demonstrated that cell-cycle-dependent phosphorylation of Mms4 by the Cdk1 and Cdc5 kinases leads to hyperactivation of Mus81-Mms4 endonuclease activity. In mitotic *S. cerevisiae* cells, Mus81-Mms4 is hyperactivated after bulk DNA synthesis has been completed. However, the basal level of Mus81-Mms4 activity appears sufficient in mitotic cells, based on the observation that a non-phosphorylatable (seven serine residues to alanine) *mms4* mutant does not exhibit hypersensitivity to DNA damage (21). Indeed, hyperactive Mus81-Mms4 activity during S-phase appears to be dangerous, possibly leading to cleavage of normal RFs and untimely DSB formation (23). The mechanism of activation by Cdk1/Cdc5-mediated phosphorylation remains to be determined.

There is significant debate regarding the substrate specificity of Mus81-Mms4 (7,24–31). The key issue is whether or not Mus81-Mms4 can act as a resolvase of intact HJs. HJs have been proposed to be direct precursors of crossovers. Crossovers are essential for proper meiosis and lead to reciprocal genetic exchange. However, crossovers can lead to loss of heterozygosity when executed between homologs in mitotic cells or can generate chromosomal translocations between ectopic recombination sites (32). Hence, it is critical for our understanding of crossover formation to determine the exact junction intermediate targeted by Mus81-Mms4. For Mus81-Mms4-dependent crossovers, we are in a position to probe the intrinsic properties of the enzyme *in vitro* that allows an extrapolation to its likely substrate(s) *in vivo*. Kinetic analysis of the substrate preference of purified *S. cerevisiae* Mus81-Mms4 has demonstrated that the enzyme can efficiently cleave a wide spectrum of DNA junctions, including 3′-flaps, RF-like structures, D-loops, nicked or partial HJs, but not intact HJs (33). The basis for this selectivity remains unclear, and there is a possibility that substrate selection is influenced by other protein partners and/or post-translational modifications. In fact, human MUS81-EME1 is associated with the nuclease scaffold SLX4, which can also bind additional nucleases such as SLX1 and XPF-ERCC1 that may engender HJ cleavage by MUS81-EME1 (34–39). In budding yeast, however, Mus81-Mms4 does not interact with Slx1-Slx4 either physically or functionally (22). Moreover, while Mus81-Mms4 nuclease activity is strongly activated by Cdk1/Cdc5 (20–23), this activation is general and does not confer latent substrate-specificity (22). Hence, further biochemical analysis is required to define the intrinsic properties of the Mus81-Mms4 endonuclease to understand its mechanism of substrate selectivity.

Here, we extend the biochemical analysis of budding yeast Mus81-Mms4 and reveal that DNA junction flexibility imparted by a nick at the branch point is an important feature for optimal nuclease activity. From these data, we inferred that Mus81-Mms4 bends its DNA substrate, and using Förster Resonance Energy Transfer (FRET) experiments, we directly demonstrate that Mus81-Mms4 induces an approximate 100° angle between two duplex arms of a 3′-flap and nicked HJ. These distortional changes in the DNA junction are accompanied by conformational changes in the protein upon selective substrate binding. Together with previously published data of substrate selectivity and mapping of Mus81-Mms4 cleavage sites (33,40–41), as well as structural information on MUS81-EME1 and other structure-selective DNA endonucleases (42–46), we propose a model for the Mus81-Mms4 catalytic cycle of DNA junction cleavage.

MATERIALS AND METHODS

Purification of Mus81-Mms4

Mus81-Mms4 and Mus81-D414A, D415A-Mms4 were purified as described (33). Crosslinking experiments employed Mus81-Mms4 protein from which the glutathion-S-transferase (GST) tag on Mms4 was removed during purification as described (22). Kinetic and FRET experiments employed heterodimer retaining the GST tag. The GST-tagged version was shown to fully complement *mus81*-Δ cells (33).

DNA substrate purification, nuclease assay and kinetic analysis

Oligonucleotides used in substrate preparation were ordered without 5′-phosphate modification (Qiagen Operon). The 5′-phosphate does not appear to affect enzyme kinetics (data not shown). DNA substrates were annealed and purified as described (33,47). Oligonucleotides for the nicked HJ structure (nXO12) are olWDH 330 (5′-CAACGTCATAGACGATTACATTG CTA CATGGAGCTGTCTAGAGGATCCGA-3′), olWDH 331 (5′-GTCGGATCCTCTAGACA GCTCCATGATC ACTGGCACTGGTAGAATTCGGC-3′), olWDH 333 (5′-TGGGTCAACGT GGGCAAAGATGTCCTAG CAATGTAATCGTCTATGACGTT-3′), olWDH 335 (5′-TGCCG AATTCTACCAGTGCCAGTGA-3′) and olWDH 336 (5′-TGGACATCTTTGCCCACGTTGA CCCA-3′); in the corresponding tethered nicked HJ structure (nXO12-linked 1–2), olWDH 335 and 336 are replaced with olWDH 519, which consists of olWDH 335 and 336 sequences linked by 25 nt of arbitrarily chosen ssDNA sequence (5′-TGGACATCTTTGCCCAC GTTGACCCATAAGCCTAGTTACGGATTACTACTT GCCGAATTCTACCAGTGCCAGTGA-3′) or olWDH 1547, with 12 nt of arbitrarily chosen ssDNA sequence (5′- GGACATCTTTG CCCACGTTGACCCATAAGCC TAGTTATGCCGAATTCTACCAGTGCCAGTGAT-3′). Oligonucleotides for the RF-like are olWDH 330, 333 and 336 as for nXO12, with olWDH 334 (5′-GTCGGATCCTCTAGACAGCTCCATG-3′); in the corresponding tethered RF-like structure (RF-like-linked), olWDH 334 and 336 are replaced with olWDH 535, which consists of olWDH 334 and 336 sequences linked by 25 nt of arbitrarily chosen ssDNA sequence (5′–TGGACA TCTTTGCCCACGTTGACCCATAAGCCTAGTTAC GGATTACTACTGTCGGATCCTCTAGACAGCTC CATG-3′). Oligonucleotides for the 3′-flapped structure (3′-flap) are olWDH 330, 331 and 336; in the corresponding tethered 3′-flap structure (3′-flap-linked), olWDH 570 (5′-ATAGACGATTACATTGCTACATGGAGCTGTCT AGAGAGCCTATCGCGAGATTACCGTGGGCAAA GATGTCCTAGCAATGTAATCGTCTAT-3′) is annealed to olWDH 572 (5′-GGACATCTTTGCCCACG-3′) to generate a hairpin loop with a duplex arms flanking the junction branch point. Oligonucleotides for the D-loop structure (labeled in Figure 1 and Table 1 as ‘D-loop (linked)’ indicating the tethered state of the substrate) are olWDH 684 (5′-CGTTGGACGCTGCC GAATTCTACCACTGCGTGCCTTGCT AGGACA TCTTTGCCCACCTGCAGGTTCACCCATCGC-3′), olWDH 685 (5′-GCGATGGG TGAACCTGCAGGTG GGCGGCTGCTCATCGTAGGTTAGTGAATTGGT AGAATTCGGCAGCGTCCAACG-3′), olWDH 686 (5′-GATCGTAAGAGCAAGATGTTCTATAAAAGA TGT CCTAGCAAGGCACGCAG-3′) and olWDH 687 (5′-TATAGAACATCTTGCTCTTACGAT C-3′); in the corresponding untethered D-loop structure, olWDH 685 is replaced with two oligonucleotides that relieve displaced ssDNA-mediated constraint between D-loop duplex arms: olWDH 723 (5′-GCGATGGGTGAACCTG CAGGTGGGCGGCTGCTCATCGT-3′) and olWDH 724 (5′-AGGTTAGTGAATTGGTAGAATTCGGCAG CGTCCAACG-3′). For fluorescently labeled substrates, oligonucleotides were purchased from Integrated DNA Technologies labeled with an internal donor fluorophore (Cy3) and/or an internal acceptor fluorophore (Cy5). The Cy3/Cy5 labeled 3′-flap (called Cy3/Cy5 3′-flap) was formed by annealing complementary oligos: olWDH 1387 (5′-TCTGACTGCAGTCG/iCy5/GGCT-3′), olWDH 1389 (5′-ACCGTCCGTCCTAGCAAGCATTCGAT-3′) and olWDH 1390 (5′-AGCCCGACTGCAGTCAGAGC TTGCTAGGACGGA/iCy3/CGGT-3′). The Cy3/Cy5 labeled nHJ (called Cy3/Cy5 nHJ) was formed by annealing complementary oligonucleotides: olWDH 1389, olWDH 1390, olWDH 1517 (5′-ACCGTCCGTCCTAGCAAGCT AGCAATGTAATCGTCTA-3′), olWDH 1518 (5′-TAGA CGATTACATTGCTACATGGAGCTGTCTAGAGGA-3′), olWDH 1519 (5′-TCCTCTAGACTGCTCCATG-3′). Nuclease assays and kinetic analysis were performed as previously described (33).

Fluorescence DNA bending assay

FRET experiments were performed in 25 mM HEPES pH 7.5, 100 mM NaCl, 1 mM DTT, 0.1 mg/mL bovine serum albumin (New England BioLabs) in the absence of 3 mM $Mg(OAc)_2$. Experiments were performed using a SLM Aminco 8100 spectrofluorometer (SLM Aminco, Inc., Urbana, IL, USA) equipped with a temperature controller set to 30°C. FRET measurements for the Cy3/Cy5 3′-flap and Cy3/Cy5 nHJ DNA substrates were performed by exciting Cy3 at 512 nm and recording Cy5 emission at 660 nm. Control experiments were conducted with Mus81-D414A, D415A-Mms4 in the presence of 3 mM $Mg(OAc)_2$. Samples were taken and transferred to stop buffer (3 mg/mL Proteinase K, 0.3% sodium dodecyl sulphate (SDS), 20 mM ethylenediaminetetraacetic acid (EDTA)) after each addition of protein, electrophoresed on 10% native polyacrylamide gel electrophoresis (PAGE) gels and visualized by Typhoon.

Determination of FRET efficiencies, fluorophore-distances and angle calculation

The efficiency of energy transfer from the donor (Cy3) to the acceptor (Cy5) fluorophore was calculated following the $(ratio)_A$ method (48). To obtain corrected efficiencies at each data point in the titration of Mus81-Mms4, the percent of protein-induced donor quenching was assessed under the same experimental conditions using a donor-only substrate.

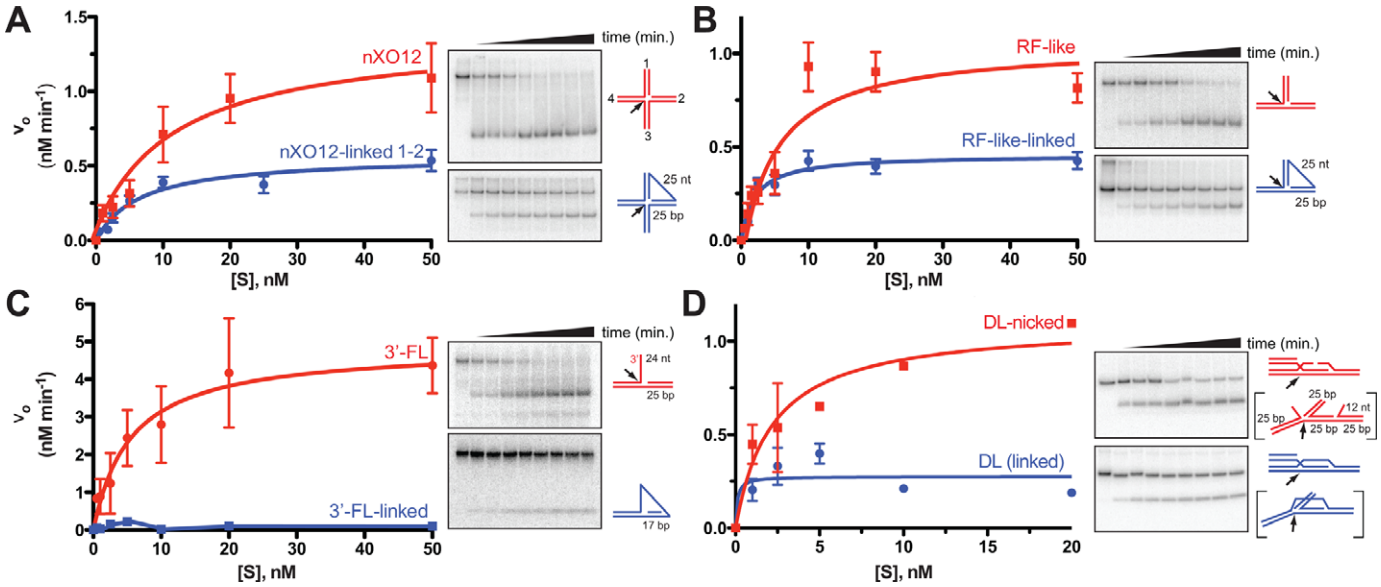

Figure 1. Mus81-Mms4 capitalizes on rotational freedom of joint DNA molecule substrate arms allowed by a phosphodiester backbone discontinuity. Michaelis–Menten plots for Mus81-Mms4 activity on joint DNA molecule substrates and tethered counterparts ('linked'). Single-stranded DNA intervening between substrate arms restricts mobility of arm rotational freedom. (A) nXO12 versus nXO12-linked 1–2 with arms 1 and 2 tethered; (B) RF-like versus RF-like-linked; (C) 3′-flap versus 3′-flap-linked; (D) D-loop versus D-loop-linked. Shown are means ± 1 SD from three independent experiments. Representative nuclease assay phosphorimages are shown (10 nM substrate), with sampling time course at 0, 3, 6, 10, 15, 20, 30, 45 and 60 min reaction time.

Table 1. Kinetic values for tethered (linked) and untethered joint DNA molecule substrates

Substrate	K_M [nM]	V_{max} nM/min]	k_{cat} [min^{-1}]	$K_M/K_{M(linked)}$	k_{cat} / $k_{cat(linked)}$
nXO12	11 ± 4.8	1.4 ± 0.2	0.3	1.7	2.3
nXO12-linked 1–2[a]	6.5 ± 1.7	0.6 ± 0.1	0.1		
RF-like	5.5 ± 1.8	1.1 ± 0.1	0.2	2.7	2.2
RF-like-linked	2.0 ± 0.5	0.5 ± 0.02	0.1		
D-loop-nicked	1.9 ± 0.9	1.1 ± 1.3	0.2	1.6	2.2
D-loop (linked)	1.2 ± 1.6	0.5 ± 0.2	0.1		
3′-flap[b]	5.5 ± 2.6	4.9 ± 0.7	1	4.6	24
3′-flap-linked	1.2 ± 1.0	0.2 ± 0.04	0.04		

[a]In this nXO12 substrate arms 1 and 2 were linked by a 24 nucleotide tether.
[b]This data are taken from ref. 33.

The corrected distance can be calculated from the equation:

$$E = 1 - F_{DA}/F_D = 1/1 + (R_{exp}/R_o)^6$$

where E is the efficiency of energy transfer, F_{DA}/F_D indicates the ratio between the donor emission at each protein concentration and in the donor-only construct, R_o represents the Förster distance in the absence of protein (54 Å), and R_{exp} is the experimental fluorophore-distance obtained following the $(ratio)_A$ method. R_{exp} can be correlated with conformational changes in the DNA substrate upon Mus81-Mms4 binding by calculating the DNA kink angle (θ) using a single-kink model (43). The kink center was assumed to be at the phosphate opposite from the ss/dsDNA junction and flanked by 14-bp (L_1 and L_2) dsDNA regions, which represent the fluorophore positions. Modeling the dsDNA arms to occupy the same plane and the inter-bp distance to be 3.4 Å (that of canonical B-DNA), the angle θ was calculated using the law of cosines for the maximal FRET vectors by the equation:

$$\cos(\theta) = [(R_{exp}^2 - L_1^2 - L_2^2)/2L_1L_2]$$

Statistical error associated with R was calculated by propagation of errors.

Mus81-Mms4 protein crosslinking on DNA joint molecules

In preparation for bis-maleimidohexane (BMH; Pierce) sulfhydryl crosslinking, purified Mus81-Mms4 aliquots were dialyzed into 20 mM Tris-HCl pH 7.5, 1 mM EDTA, 10% glycerol with 150 mM NaCl. Protein concentration was then re-determined by Bradford assay. Crosslinking reactions contained 250 nM Mus81-Mms4 and 250 nM DNA junctions, in 10 μl of buffer containing 25 mM Tris-HCl pH 7.0, 150 mM NaCl and 5 mM EDTA. After 3 min incubation at room temperature, 0.5 μl of BMH (in dimethyl sulfoxide (DMSO)) was added to a final concentration of 50 μM. Reactions lacking BMH received 0.5 μl DMSO. After 10 additional minutes at room temperature, the reactions

were stopped with the addition of 0.5 μl 0.5 M dithiothreitol (DTT). After heating in Laemmli buffer, sample volumes corresponding to 25 ng crosslinked heterodimer or 5 ng uncrosslinked samples were separated on 4–12% tris-glycine SDS-PAGE gels (Lonza) followed by transfer to nitrocellulose membranes at 400 mA for 80 min. Membranes were immunoblotted with rat anti-Mms4 serum, stripped and reprobed with rabbit anti-Mus81 serum.

RESULTS

Mus81-Mms4 requires DNA junction flexibility

To explain the innate preference of the budding yeast Mus81-Mms4 endonuclease for nicked DNA junctions, we reasoned that a backbone discontinuity intrinsic to a substrate branch point allows rotational freedom of DNA arms. HJs can adopt different conformations from square planar in the absence of divalent cations to two different stacked X structures in the presence of divalent cations (49,50). However, among all substrates discussed here, the HJ is the only junction molecule with highly restricted rotational freedom due to the lack of a discontinuity (nick/gap) at the junction branch point. Inherent rotational freedom may allow Mus81-Mms4 to interpret substrate properties during enzyme conformational changes associated with DNA junction binding and catalysis. DNA bending by conformational changes associated with substrate 'sampling' may also store energy in the bent DNA that can be used, in turn, to induce activating conformational changes in the enzyme (51).

To test whether substrate bending is relevant to Mus81-Mms4 substrate processing, kinetic analysis was performed on substrates with physically restricted DNA arms in three model joint molecules (nXO12, RF-like and 3′-flap structures) and with relieved inherent strain in one model joint molecule (D-loop structure) (Figure 1 and Table 1). In all cases where DNA arms were tethered, both K_M and k_{cat} were reduced relative to standard untethered. For nXO12 with arms 1 and 2 (nXO12-linked 1–2) tethered by a 24 nt linker, both K_M and k_{cat} are reduced approximately 2-fold. Reducing the length of the tether to 12 nt gave identical results to the 24 nt tethered substrate (data not shown).

For the RF-like substrate with tethered arms, KM is reduced nearly 3-fold and kcat is reduced approximately 2-fold and (Figure 1 and Table 1). Both KM and kcat are reduced on tethered nXO12 and RF-like junctions (Table 1).

Tethering DNA arms on the 3′-flapped substrate nearly abolishes its cleavage. This could be related to the reduced arm length on the tethered 3′-flap (17 bp as opposed to 25 bp on the untethered 3′-flap), although the fluorescently labeled 3′-flap (see Supplementary Figure S3) with 18 bp arms is cleaved with the same k_{cat} as the 3′-flap with 25 bp arms ((33), data not shown). The arm length was reduced on the tethered 3′-flap because of limits to the maximum synthetic oligonucleotide length available). The tethered 3′-flap is the only substrate where the cleaved arms are linked. To test whether this feature determines the extremely low cleavage efficiency of the linked 3′-flap, we tethered the cleaved arms 1 and 3 of the nHJ (nXO12-linked 1–3; Supplementary Figure S1). The results showed a 4-fold reduction in K_M and k_{cat} for the substrate with a 24 nt tether and a similar reduction when the tether was shortened to 12 nt (Supplementary Figure S1). These data suggest that the change in position of the tether has no major influence. [The data presented in Figure 1 and Table 1 and Supplementary Figure S1 were separated by several years using different enzyme and substrate preparations, which accounts for the variation in the kinetic parameters for the nXO12 junction between sets of experiments.]

In a converse scenario, duplex arm rotational freedom at the junction branch point is inherently restricted in model D-loop substrates, where the D-loop ssDNA tethers arms upstream of the branch point to the downstream arm. K_M and k_{cat} are raised when the intrinsic D-loop constraint is relieved by constructing the D-loop ssDNA with two separate oligonucleotides (Figure 1 and Table 1), consistent with the observation that constraint of duplex arm rotational freedom at a substrate branch point interferes with catalytic processing by Mus81-Mms4.

All five substrate pairs show a consistent trend that reducing arm flexibility leads to better substrate binding (lower K_M) but interferes with catalysis (lower k_{cat}). These observations suggest that Mus81-Mms4 conformational states associated with substrate binding, catalysis of phosphodiester bond hydrolysis, and/or substrate release are coupled to duplex arm mobility and arm bending relative to a vertex defined by the junction branch point.

Consistent with the view that Mus81-Mms4 cleavage is largely determined by the presence and position of two duplex arms flanking a strand discontinuity, changes in the length of the third strand emanating from the junction has relatively small consequences on cleavage efficiency (Supplementary Figure S2). In 3′-flaps, this arm is single-stranded DNA, whereas in RF-like substrates this arm is duplex DNA (Supplementary Figure S2). For both 3′-flap and RF-like substrates, the structures with the shortest arms are cleaved best. Interestingly, nicked duplex DNA is also cleaved to a significant degree, although not to the extent of flaps with even the shortest additional ssDNA or dsDNA arm at the branch point (Supplementary Figure S2). In contrast, duplex DNA that transitions to exclusively ssDNA at the branch point (3′-tailed DNA) is essentially not cleaved, nor can duplex DNA without a nick be incised (33). These differences relative to nicked duplex DNA underline the necessity for two duplex DNA arms flanking a flexible branch point as a fundamental requirement for Mus81-Mms4 substrate recognition.

Mus81-Mms4 bends cleavable DNA junctions

The dependence of Mus81-Mms4 on DNA junction flexibility suggests that the enzyme bends its substrate. To directly test whether Mus81-Mms4 induces substrate bending, we designed a 3′-flap where both duplex arms contained fluorophores positioned to conduct FRET experiments (Figure 2A). Because the dsDNA arms of this Cy3/Cy5 3′-flap are well below the 150 bp persistence length of dsDNA (52), this substrate permits distance estimates to be calculated between the two fluorophores. Three properties of the Cy3/Cy5 3′-flap make it amenable to FRET efficiency analysis: (1) both fluorophores are positioned on the ds-

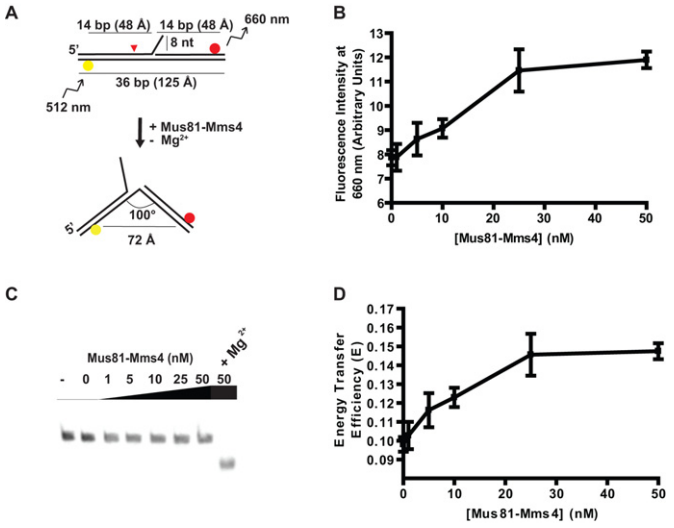

Figure 2. Mus81-Mms4 binding to 3′-flap substrates kinks Cy3/Cy5-labeled duplex arms flanking the branch point up to 100°. (A) Schematic of FRET bending assay with the Cy3/Cy5 3′-flap substrate, where excitation of the Cy3 (yellow) donor (λ_{ex} = 512 nm) within close proximity to Cy5 (red) acceptor (λ_{em} = 660 nm) leads to energy transfer when protein-induced kinking occurs in the absence of Mg^{2+}. Changes in inter-fluorophore distance caused by Mus81-Mms4 bending of the dsDNA arms in the Cy3/Cy5 3′-flap substrate flanking the branch point discontinuity are indicated. (B) Fluorescence emission by Cy5 (λ_{em} = 660 nm) upon Mus81-Mms4 addition to 10 nM Cy3/Cy5 3′-flap in the absence of Mg^{2+}. (C) Representative native PAGE images of DNA substrates and cleavage products after Mus81-Mms4 titration and subsequent Mg^{2+} addition. (D) FRET efficiency upon Mus81-Mms4 addition to 10 nM Cy3/Cy5 3′-flap in the absence of Mg^{2+}. Shown are means ± 1 SD from three independent experiments.

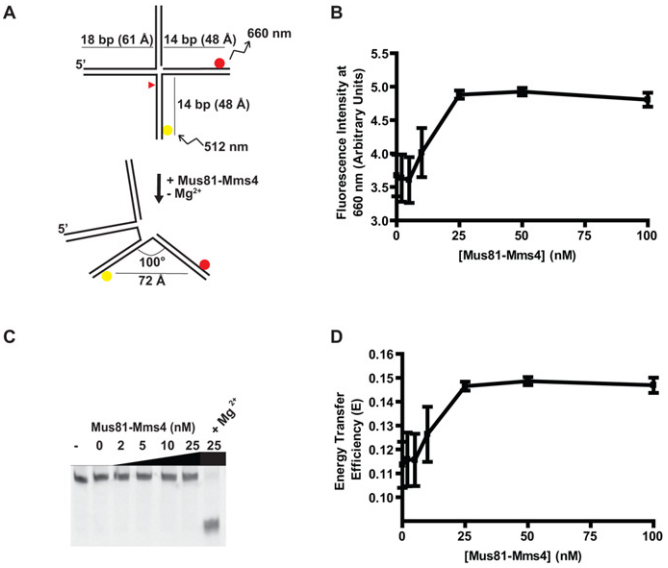

Figure 3. Mus81-Mms4 binding to nicked HJ joint DNA molecule kinks Cy3/Cy5-labeled duplex arms flanking the branch point up to 100°. (A) Schematic of FRET bending assay with the Cy3/Cy5 nHJ substrate, where excitation of the Cy3 (yellow) donor (λ_{ex} = 512 nm) within close proximity to Cy5 (red) acceptor (λ_{em} = 660 nm) leads to energy transfer when protein-induced kinking occurs in the absence of Mg^{2+}. Changes in inter-fluorophore distance caused by Mus81-Mms4 bending of the dsDNA arms in the Cy3/Cy5 nHJ substrate flanking the branch point discontinuity are indicated. (B) Fluorescence emission by Cy5 (λ_{em} = 660 nm) upon Mus81-Mms4 addition to 5 nM Cy3/Cy5 nHJ in the absence of Mg^{2+}. (C) Representative native PAGE analysis of DNA substrates and cleavage products after Mus81-Mms4 titration and subsequent Mg^{2+} addition. (D) FRET efficiency upon Mus81-Mms4 addition to 5 nM Cy3/Cy5 nHJ in the absence of Mg^{2+}. Shown are means ± 1 SD from three independent experiments.

DNA arms surrounding the junction and strand discontinuity, and (2) the fluorophores are positioned at a distance that allows accurate measurement of changes in fluorophore-distance as a function of FRET efficiency change and (3) the fluorophores do not significantly affect the Mus81-Mms4 Michaelis–Menten kinetics (See Figure 2C, Supplementary Figure S3). By measuring changes in the fluorescence intensity of the Cy5 (FRET acceptor) peak upon excitation of Cy3 (FRET donor), we determined the distance in solution between the two fluorophores in the absence and presence of Mus81-Mms4 (Table 2). Upon Mus81-Mms4 titration into reactions with 10 nM Cy3/Cy5 3′-flap, there was a 51% increase in peak emission of Cy5 (Figure 2B). The protein-induced FRET efficiency was 0.15 ± 0.004 for 10 nM Cy3/Cy5 3′-flap, corresponding to an inter-fluorophore distance of 72 ± 0.2 Å (Figure 2D, Table 2). Experiments with 5 nM Cy3/Cy5 nHJ confirmed these results (data not shown). Control experiments demonstrated that the Cy3/Cy5 3′-flap was cleaved by Mus81-Mms4 after addition of Mg^{2+} (Figure 2C). Catalytic deficient Mus81-D414A, D415A-Mms4 in the presence of Mg^{2+} displayed a similar 56% increase in Cy5 emission upon protein titration with 10 nM Cy3/Cy5 3′-flap (Supplementary Figure S4A, Table 2) and a similar increase in protein-induced FRET efficiency to 0.13 ± 0.013, corresponding to an inter-fluorophore distance of 74 ± 0.8 Å (Supplementary Figure S4B, Table 2). The fluorescence intensity of 10 nM Cy3-only (Supplementary Figure S4C) or Cy5-only (Supplementary Figure S4D) 3′-flap substrates remains constant over the 5-min sampling time (data not shown), independent of protein concentration and the emission spectra of Cy3 (Supplementary Figure S4E) and Cy5 (Supplementary Figure S4F) do not change in the presence of Mus81-Mms4 at 5-fold excess to substrate. Therefore, Mus81-Mms4 binding does not quench the donor or acceptor fluorophore emissions, and the change in fluorescence intensity reflects changes in energy transfer caused by decreasing inter-fluorophore distance (Figure 2D, Table 2). Under the assumption that Mus81-Mms4 bends duplex arms of the 3′-flap at a vertex defined by the phosphodiester bond opposite the flap junction, and taking into account the position of the fluorophores and the helical structure of B-form DNA, these results suggest that Mus81-Mms4 binding induces a kink at the branch point discontinuity that positions the duplex arms at an angle of 100° (Figure 2A, Table 2). This angle estimate assumes bending in a single dimension without torsional twist.

To test whether substrate bending is a general characteristic of Mus81-Mms4, we established the fluorescence-based bending assay with a Cy3/Cy5 nHJ (Figure 3A) where the fluorophores are placed in analogous positions to those in the Cy3/Cy5 3′-flap. The presence of fluorophores does not affect Mus81-Mms4 Michaelis–Menten kinetics (Supplementary Figure S5). Upon Mus81-Mms4 titration

Table 2. Summary of FRET measurements with Cy3/Cy5 substrates

Sample	Energy transfer efficiency	Fluorophore distance[d] (Å)	Calculated angle (°)	Figure reference
3′-flap	0.098 ± 0.004	78 ± 0.3	100	2
3′-flap + WT [a, b]	0.147 ± 0.004	72 ± 0.2		
3′-flap	0.088 ± 0.008	80 ± 0.6	101	S4
3′-flap + DD [a, b]	0.133 ± 0.013	74 ± 0.8		
nHJ	0.114 ± 0.010	76 ± 0.6	100	3
nHJ + WT [a, c]	0.147 ± 0.003	72 ± 0.2		
nHJ	0.108 ± 0.007	77 ± 0.5	101	S6
nHJ + DD [a, c]	0.139 ± 0.005	73 ± 0.3		

[a]WT: Mus81-Mms4; DD: Mus81-D414A, D415A-Mms4.
[b]10 nM Cy3/Cy5 3′-flap + 50 nM heterodimer.
[c]5 nM Cy3/Cy5 nHJ + 100 nM heterodimer.
[d]Distances calculated using Förster distance (R_o) of 54 Å.

into reactions containing 5 nM Cy3/Cy5 nHJ, there was a 31% increase in peak emission of Cy5 (Figure 3B). The protein-induced FRET efficiency was 0.15 ± 0.003 for 5 nM Cy3/Cy5 nHJ, corresponding to an inter-fluorophore distance of 72 ± 0.2 Å (Figure 3D, Table 2). Control experiments demonstrated that the Cy3/Cy5 nHJ was cleaved by Mus81-Mms4 after addition of Mg^{2+} (Figure 3C). Catalytic deficient Mus81-D414A, D415A-Mms4 in the presence of Mg^{2+} displayed a similar increase in protein-induced FRET efficiency to 0.14 ± 0.003, corresponding to an inter-fluorophore distance of 73 ± 0.3 Å (Supplementary Figure S6, Table 2). The substrate fluorescence intensity was not affected by sampling time or the presence excess Mus81-Mms4 (Figure 3D, Supplementary Figure S6, C–E, Table 2). In striking similarity to the 3′-flap substrate, the results suggest that Mus81-Mms4 also bends the nHJ at an angle of 100° (Figure 3A, Table 2).

The fluorescence-based assay was also conducted with an intact Cy3/Cy5 HJ (Supplementary Figure S7A). Upon Mus81-Mms4 addition in the absence of Mg^{2+} (Supplementary Figrue S7B) or Mus81-D414A, D415A-Mms4 in the presence of Mg^{2+} (Supplementary Figure S7D), there was no increase in peak emission of Cy5. Instead, there was a decrease in emission, which was also evident in the emission spectra of Cy5 (data not shown). Such a signal decrease would be consistent with Mus81-Mms4 binding causing the dsDNA arms labeled with fluorophores to splay further apart from each other. Control experiments demonstrated that the Cy3/Cy5 HJ was not cleaved by Mus81-Mms4 after addition of Mg^{2+} (Supplementary Figure S7C). Importantly, these results taken together with the Cy3/Cy5 3′-flap and Cy3/Cy5 nHJ results indicate that Mus81-Mms4 relies on substrate flexibility for efficient bending and cleavage of its DNA substrates.

Substrate-dependent conformational change of Mus81-Mms4

As proteins transition between alternate conformational states, different quaternary domains and amino acid residues become exposed and juxtaposed. Using chemical crosslinking agents with two functional groups separated by defined spacing (bifunctional), it is possible to detect such conformational changes by differences in the crosslinking patterns. Mus81 and Mms4 contain 12 and 7 cysteine residues, respectively, lending ample opportunity to detect differential crosslinking patterns with a thiol crosslinker. We employed the bifunctional thiol crosslinker, BMH, which has two reactive maleimide groups separated by a 13 Å hexane linker, to crosslink protein to protein but not protein to DNA (53). Adding BMH to Mus81-Mms4 in solution followed by SDS–PAGE and immunoblot analysis revealed a species that electrophoreses corresponding to a relative mobility ∼200 kDa (Figure 4 lane 2, species labeled ‘DNA-independent’). This mobility is consistent with a crosslinked heterodimer (156 kDa) with slower migration due to the covalent thiol crosslinking, which does not allow the denatured proteins to fully extend into rod-like SDS–amino acid chains. Both subunits of the heterodimer were confirmed to be present in these complexes by immunoblotting for Mms4 (Figure 4A) and Mus81 (Figure 4B). Next, Mus81-Mms4 was pre-bound to a number of joint DNA molecule structures and then crosslinked with BMH. Surprisingly, novel faster-migrating Mus81-Mms4 crosslinked species appeared after crosslinking in the presence of a subset of DNA structures (Figure 4, bands labeled ‘DNA-dependent’). Consistent between several experiments, the same crosslinked-heterodimer electrophoretic mobility patterns were observed for the various DNA structures. Interestingly, two distinct DNA-dependent species with slightly different mobilities were discerned. The 3′-flap-induced novel crosslinked species is slower-migrating than the species induced by the 5′-flap. The same flap polarity relationship of crosslinked species is seen for structures with three duplex arms and single-stranded DNA of defined polarity at the branch point (pX012–3′ and pX012–5′). In summary, slower-migrating crosslinked species correlate with DNA junctions that have a 5′ end at the branch point such as a 3′-flap, and the faster-migrating species correlate with DNA junctions that have a 3′ strand end (3′-OH) at the branch point, such as a 5′-flap. The migration patterns of all experimentally examined DNA structures are summarized in Table 3. All of the DNA structures that induced a DNA-dependent crosslinked species, be it the faster or slower migrating

Table 3. Summary of DNA structure-induced novel crosslinked species

Slower-migrating DNA-dependent band	**Faster-migrating** DNA-dependent band	**No** DNA-dependent band
3′-flap (3)[a]	5′-flap (4)	X012 (7)
pX012 3′ (5)	pX012 5′ (6)	X12 (8)
D-loop (10)	Nicked X012 (9)	Y junction (12)
	RF-like (11)	
5′ only at junction	3′ only or both 3′ **and** 5′ at junction	**No** strand end at junction (Y) or contiguous (HJs)

[a]The number in brackets indicates the lane number in Figure 4.

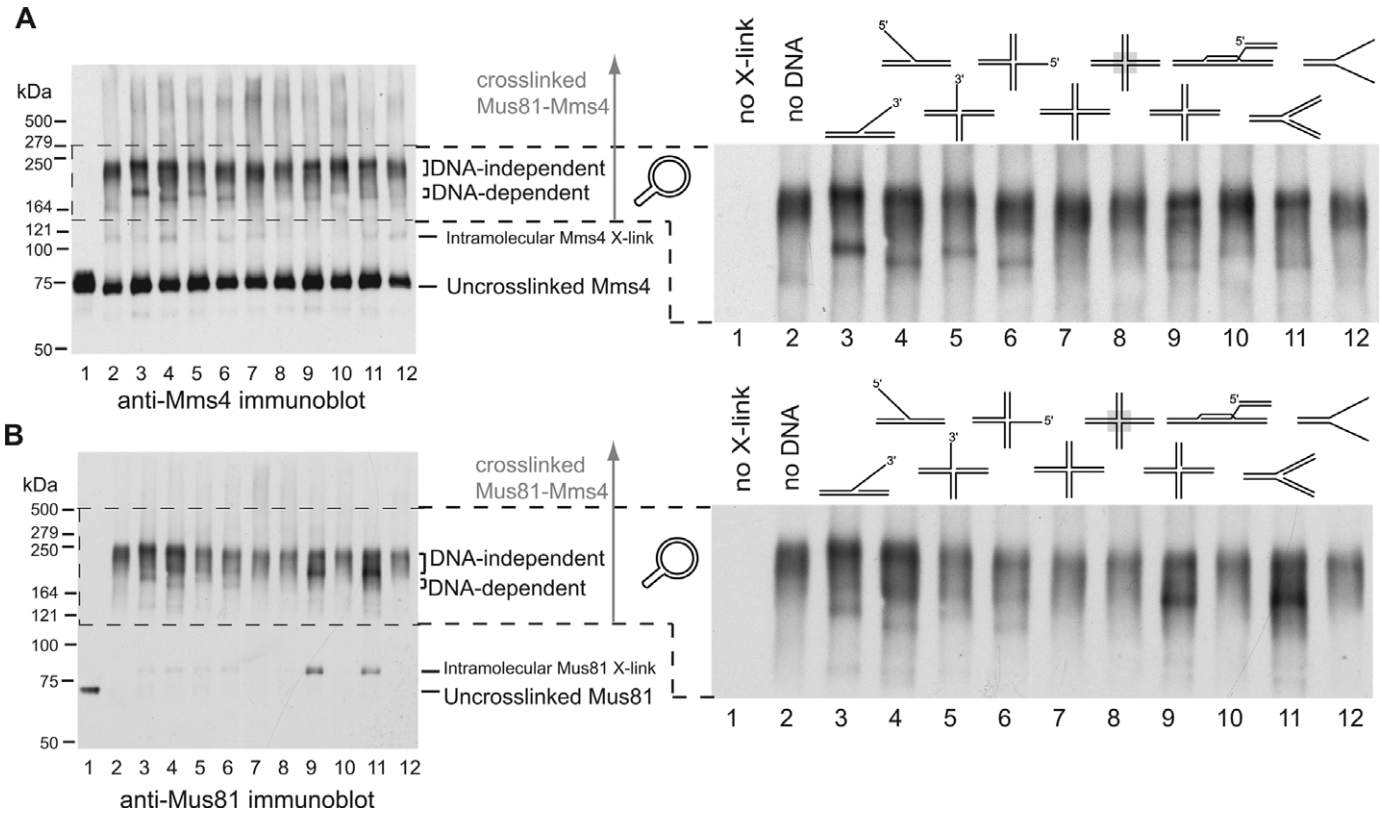

Figure 4. Thiol-crosslinking of Mus81-Mms4 bound to joint DNA molecules reveals DNA structure-induced conformational changes in Mus81-Mms4. 250 nM Mus81-Mms4 was bound to 250 nM DNA junctions. The structures are lane 3: 3′ flap; lane 4: 5′ flap; lane 5: partial X junction-3′ (pX012–3′); lane 6: partial X junction-5′ (pX012–5′); lane 7: X junction with non-mobile core (X012); lane 8: X junction with 12 bp/arm migrateable core (X12); lane 9: X012 with a nick near the center of the structure (nX012); lane 10: D-loop mimic; lane 11: RF-like; and lane 12: simple Y. For sequences of component strands, see (47)). After 3-min incubation of Mus81-Mms4 with DNA junctions, 50 μM crosslinker (BMH) in 0.5 μl DMSO (or DMSO alone for no crosslink control) was added for 10 min at 23 °C. Crosslinking reactions were stopped with DTT, electrophoresed by standard SDS-PAGE and immunoblotted (25 ng heterodimer/lane) using (A) rat anti-Mms4 and (B) rabbit anti-Mus81 sera. The same blot was probed by both antibodies and is representative of three independent experiments. The anti-Mms4 antiserum showed much higher affinity that the anti-Mus81 antiserum, which is particularly evident for the uncrosslinked protein bands.

form, have DNA discontinuities at the branch point and are cleaved catalytically (multiple junctions turned over per heterodimer) by Mus81-Mms4, with K_M values between 1.2 and 7.3 nM and k_{cat} values from 0.1 to 1.4 min^{-1} (33). The DNA structures that did not show the novel crosslinked species either did not have any dsDNA on the arm opposite the branch point (Y structure) or contained junctions without a strand discontinuity (X12 and X012). The Y structure is one of the poorest substrates incised by the heterodimer, yet cleavage is still catalytic and kinetic values can be measured (K_M = 30.1 nM), whereas the two intact HJs are incised so poorly that their kinetic values cannot be determined (33). Thus, nuclease activity on DNA junction structures correlates with the ability of the structure to induce differentially crosslinked forms of Mus81-Mms4. This suggests that Mus81-Mms4 undergoes a conformational change on DNA that is separate from initial DNA binding, and which is influenced by the nature of DNA features at the DNA junction branch point discontinuity.

DISCUSSION

Here we provide a rationale for the substrate selectivity of the Mus81-Mms4 endonuclease by combining three independent experimental approaches that lead us to the following conclusions. First, Mus81-Mms4 has a minimum requirement for two duplex arms flanking a strand dis-

continuity (nick, ss-dsDNA junction) as deduced from the cleavage of a nicked duplex but the failure to process duplex DNA or 3′-tailed DNA (Supplementary Figure S2, (33)). The previously documented difference between efficient cleavage of RF-like substrates (2–3 duplex arms) and poor cleavage of a Y junction (single duplex arm) (33) provides additional support for this point. Second, Mus81-Mms4 has high tolerance for variation in the length and structure of a third arm (ssDNA or dsDNA) at the junction (Supplementary Figure S2) as well as the presence of a fourth arm (33). This tolerance also suggests that Mus81-Mms4 could be suited to cleave substrates with proteins, such as type 1 topoisomerases, covalently attached to the 3′-end of an ssDNA flap. This would be consistent with the extreme sensitivity of yeast *mus81* mutants to the topoisomerase I poison CPT, which traps 3′-covalently linked Topoisomerase I-DNA complexes (1,54). However, it is also possible that Mus81-Mms4/EME1 targets stalled RFs that form in response to CPT treatment (19). Third, optimal cleavage by Mus81-Mms4 requires DNA junction flexibility and substrate conformational change (Figure 1, Table 1). The lower K_M on substrates with tethered arms suggests that a subset of DNA arm dispositions may promote junction binding, but the reduced k_{cat} indicates that secondary DNA binding events or deformations associated with catalysis may be required to complete an incision cycle. This agrees with a model derived from a crystal structure of a chimeric zebrafish/human MUS81-EME1 complex, where a nHJ was modeled into the active site. It appeared that several basic residues outside the active site coordinated phosphate groups of a flexible duplex arm. This positions the scissile phosphodiester bond linking the fourth and fifth nucleotides 5′ of the branch point/nick in the catalytic site. It was hypothesized that the "hinge-bending" domain between the helix-hairpin-helix (HhH2) motif and the nuclease domain can facilitate this extreme DNA bending (46). Fourth, Mus81-Mms4 bends flexible DNA junctions to an angle of about 100° around the branch point (Figures 2 and 3, Supplementary Figures S4, S6; Table 2; see below for discussion). Fifth, Mus81-Mms4 itself undergoes substrate-specific conformational changes during its catalytic cycle (Figure 4). The orientation of the strands immediately in the vicinity of the branch point influences k_{cat} (33) and two different crosslinking events take place depending on the polarity of the DNA strand end at the junction and possibly additional substrate features. This suggests that the conformational change induced by DNA junctions with the same general structure but opposite strand polarities is not equivalent. However, the site of strand incision, defined by the position of the branchpoint adjacent to the strand discontinuity, remains unchanged at four nucleotides upstream of the branchpoint (40) regardless of junction strand polarities (e.g. 3′-flap versus 5′-flap and pX012–3′ versus pX012–5′ are DNA junction pairs that have identical gross structures but opposite strand polarities, yet retain the same incision points relative to the branchpoint). These observations suggest that the site of incision is determined by the gross structure of the DNA junction, but that catalysis is influenced by finer junction features such as strand polarities, as evident by differences in catalysis (33) based on this criteria and different conformational changes captured by the crosslinked species in this study. The direct interaction of Mus81-Mms4 with the junction discontinuity and the induced conformational changes in Mus81-Mms4 when bound to cleavable substrates, but lacking for HJs, is yet further evidence that the *in vivo* substrate of this enzyme is likely a nicked junction and unlikely an intact HJ.

DNA bending: a common theme in structure-selective endonucleases and other DNA metabolic enzymes

Based on previously established substrate selectivity data for Mus81-Mms4 (33), we reasoned that a nick adjacent to a junction branch point allows duplex arms rotational freedom. Substrate deformation during recognition or catalysis is common to proteins that act on DNA, and DNA bending may be a structure-recognition mechanism universal to XPF-like and other structure-selective endonucleases. The crystal structure of *Aeropyrum pernix* XPF indicated that in order for both HhH2 domains of XPF to engage the ds-DNA arms of the substrate, there would have to be a 90° kink in the DNA (55). Substrate bending was confirmed by FRET analysis that showed that XPF kinks the DNA and was stimulated by PCNA (42). The *Archaeoglobus fulgidus* FEN1 crystal structure and FRET analysis provided evidence for DNA-dependent protein conformational changes where the α2–α3 helical loop movements provide ordering interactions with the adjacent α4–α5 helical clamp to promote a newly formed, packed anti-parallel two-helix bundle that closes over the active site to facilitate substrate-selective catalysis (43). This is in agreement with the *Homo sapiens* FEN1 crystal structure with DNA, which indicates that sharply bent DNA molecules are recognized by the nuclease by four structural elements that compose a glove-like structure: (1) an α2–α3 organized loop interacting with upstream and downstream dsDNA like a glove, (2) a 3′-flap binding pocket like a thumb and forefinger, (3) a helix-two turn-helix (H2TH) domain that interacts with downstream DNA like a wrist and (4) a two-metal ion active site that cleaves the 5′-flap ssDNA between the thumb and the finger (44). *Homo sapiens* EXO1 displayed a very similar catalytic mechanism where two helical structures were bound by H2TH domains and there was a fray in the DNA, positioning the scissile phosphodiester bond two nucleotides from the junction in the catalytic site (45). Taken together, these data suggest a common mechanism by which Mus81-Mms4 and other DNA structure-selective nucleases recognize and incise their cognate substrates through DNA bending (56). Substrate bending may store binding energy that may drive downstream conformational changes of the enzymes during the catalytic cycle (Figure 5).

Beyond DNA structure-selective nucleases, DNA substrate bending appears to be common to multiple, evolutionarily diverse families of DNA metabolic enzymes. The eubacterial mismatch recognition factor MutS, for example, bends DNA as part of its search mode for DNA mismatches (51). The potential energy stored in the bent DNA may be transferred to a conformational change in MutS, which activates later steps in the mismatch repair pathway. *S. cerevisiae* Top2 induces a 150° bend in its gate-DNA substrate, associated with substantial conformational changes that facilitate nucleophilic attack on the phosphodiester backbone

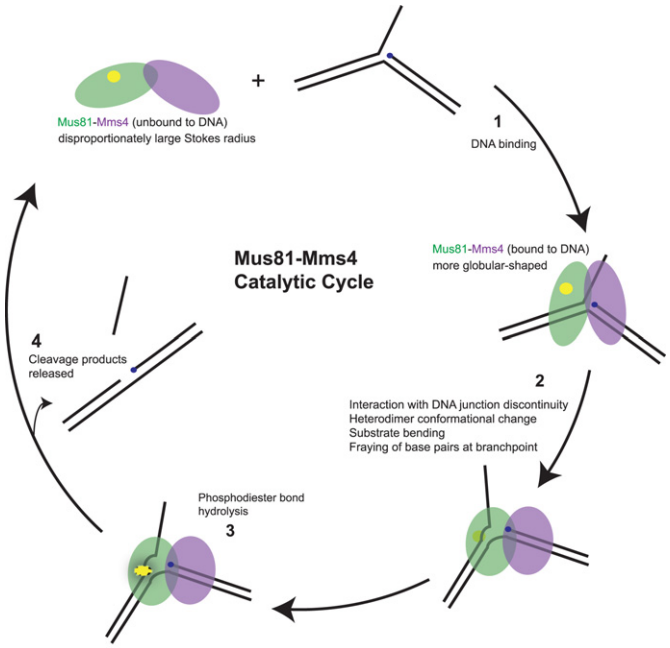

Figure 5. The catalytic cycle of Mus81-Mms4 involves DNA junction discontinuity recognition, substrate bending, and protein conformational changes. Mus81-Mms4 sampling of joint DNA junctions entails (1) beinding of DNA duplex arms flanking a backbone discontinuity, and the adoption of a more globular heterodimer shape relative to its significantly non-globular shape in solution (yellow circle represents the nuclease active site on Mus81 and the DNA end at the junction is indicated by a blue dot). (2) Mus81-Mms4 interaction with duplex DNA flanking the branch point (up to and including direct interaction with the DNA backbone discontinuity) leads to substantial kinking of DNA at a vertex defined by the branch point; substrate bending may be coupled to a secondary conformational change in the heterodimer as well as melting of four base pairs upstream from the junction branch point, which (3) positions the nuclease domain to direct hydrolysis of the phosphodiester bond between the fourth and fifth upstream nucleotides. (4) Product release completes the catalytic cycle. For simplicity the 3′-flap substrate is shown, but the model is intended to all cleavable substrates and substrate bending was verified for the nHJ substrate.

(57). So severe is the distortion in the Top2-gate DNA complex that DNA in the catalytic center is transitioned to A-form structure. In these examples, the enzyme is adapted to mechanical properties of its DNA substrate, which can be bent to an angular and rotational orientation accommodated or enforced by a conformational change in the protein complex. Compatibility to bending alters presentation of scissile bonds and promotes responsive conformational changes in the enzyme that lead to catalysis (51).

A model for the catalytic cycle of Mus81-Mms4

In Figure 5, we integrate kinetic ((33,40–41); this study), hydrodynamic (22,30), crosslinking (this study) and structural data (46) available for Mus81-Mms4/MUS81-EME1 into a model for the catalytic cycle of Mus81-Mms4 using the 3′-flap substrate for illustration. Initial DNA junction binding is based on recognition of the minimal characteristics of two duplex arms flanking a branch point. Hydrodynamic analysis suggests that interaction with the DNA junction induces a conformational change in the heterodimer upon DNA binding. Mus81-Mms4 exhibits a larger Stokes radius and smaller sedimentation coefficient than typical for a globular complex of its molecular weight, indicating that the heterodimer has a non-globular shape (22,30). Interestingly, the sedimentation coefficients of the heterodimer bound to 3′-flap or HJ structures were very close to what is expected for a complex with *globular* dimensions (22). This suggests that Mus81-Mms4 adopts a more compact conformation upon DNA binding. HJs (cleaved poorly, relatively inflexible) and 3′-flaps (cleaved catalytically, flexible at the branch point) both showed this effect in experiments conducted in the absence of the essential cofactor Mg^{2+} to prevent substrate cleavage, demonstrating that the compaction occurs before catalysis. Upon junction binding, Mus81-Mms4 induces a 100° bend across the substrate branch point that we suggest is associated with the DNA-dependent conformational change of Mus81-Mms4 observed by thiol crosslinking. The dependence of the different crosslinked species on the nature of the DNA junction strand polarities suggests that the enzyme interacts with the discontinuous DNA strand abutting the junction downstream of the branch point (DNA immediately adjacent to the nick itself). We surmise from Mus81-Mms4 cleavage site analysis (40) and in analogy to XPF, FEN1 and EXO1 (44,45) that Mus81-Mms4 frays the duplex DNA upstream of the junction branch point/nick to prepare the substrate for phosphodiester bond hydrolysis between the fourth and fifth nucleotide 5′ to the junction branch point. The incision product is rendered with a four-nucleotide gap that cannot be directly ligated to DNA downstream of the branch point.

In summary, we have presented observations that collectively suggest that Mus81-Mms4 induces conformational changes in its DNA substrates, coupled to conformational changes in the heterodimer itself. Each conformational state detected depends on the presence of a nick intrinsic to the DNA junction branch point, meaning that a DNA backbone discontinuity is significant to optimal substrate recognition and processing of joint molecules by Mus81-Mms4. Hence, the strand discontinuity is important both for its capacity to confer duplex arm rotational freedom at the junction branch point and also for its presentation of an exposed end adjacent to the nick that correlates with novel enzyme conformational states on DNA junctions competent for catalytic incision. The exposed DNA strand downstream of the branch point nick may be directly detected and bound by Mus81-Mms4, as it affects catalysis (40). HJs are poor *in vitro* substrates because of limited arm rotational freedom and the lack of interaction with this secondary DNA binding site. *In vivo*, limitations to HJ arm rotational freedom may be overcome by junction incision by other nucleases or by DNA structural conformations imposed by other proteins specific to a recombination pathway. Although our studies do not preclude the intact HJ as an *in vivo* substrate for Mus81-Mms4, they indicate that features fundamental to the four-way junction may pose high energetic barriers to the substrate deformations necessary for incision. Our results and conclusions are in good agreement with recent structural studies from Dr Yunje Cho's laboratory (Pohang University of Science and Technology, Pohang, South Korea) with human MUS81-EME1 [Gwon G.H *et al.*

(2014) Crystal Structures of the structure-selective nuclease Mus81-Eme1 bound to flap DNA substrates. EMBO J. in press].

SUPPLEMENTARY DATA

Supplementary Data are available at NAR Online.

ACKNOWLEDGEMENTS

We thank Steve Kowalczykowski and Neil Hunter for sharing equipment, and Yunje Cho for sharing unpublished results. S.M. specially thanks Chris Dombrowski and Jessica Chau for help with FRET experiments.

FUNDING

National Institutes of Health (NIH) [GM58015 and CA92276 to W.D.H.]; NIH T32 Molecular & Cellular Biology [T32 GM007377 to K.T.E.]; Tobacco-Related Disease Research [20DT-0036 to S.M., 17DT-0178 to W.D.W.]; NIGMS T32 Pharmacology: Bench to Bedside [T32 GM099608 to S.M.]. Funding for open access charge: NIH [GM58015].
Conflict of interest statement. None declared.

REFERENCES

1. Boddy,M.N., Lopez-Girona,A., Shanahan,P., Interthal,H., Heyer,W.D. and Russell,P. (2000) Damage tolerance protein Mus81 associates with the FHA1 domain of checkpoint kinase Cds1. *Mol. Cell. Biol.*, **20**, 8758–8766.
2. Interthal,H. and Heyer,W.D. (2000) MUS81 encodes a novel Helix-hairpin-Helix protein involved in the response to UV- and methylation-induced DNA damage in Saccharomyces cerevisiae. *Mol. Gen. Genet.*, **263**, 812–827.
3. Dendouga,N., Gao,H., Moechars,D., Janicot,M., Vialard,J. and McGowan,C.H. (2005) Disruption of murine Mus81 increases genomic instability and DNA damage sensitivity but does not promote tumorigenesis. *Mol. Cell Biol.*, **25**, 7569–7579.
4. Hanada,K., Budzowska,M., Modesti,M., Maas,A., Wyman,C., Essers,J. and Kanaar,R. (2006) The structure-specific endonuclease Mus81-Eme1 promotes conversion of interstrand DNA crosslinks into double-strands breaks. *EMBO J.*, **25**, 4921–4932.
5. Mazina,O.M. and Mazin,A.V. (2008) Human Rad54 protein stimulates human Mus81-Eme1 endonuclease. *Proc. Natl. Acad. Sci. U.S.A.*, **105**, 18249–18254.
6. Matulova,P., Marini,V., Burgess,R.C., Sisakova,A., Kwon,Y., Rothstein,R., Sung,P. and Krejci,L. (2009) Cooperativity of Mus81.Mms4 with Rad54 in the resolution of recombination and replication intermediates. *J. Biol. Chem.*, **284**, 7730–7742.
7. Hickson,I.D. and Mankouri,H.W. (2011) Processing of homologous recombination repair intermediates by the Sgs1-Top3-Rmi1 and Mus81-Mms4 complexes. *Cell Cycle*, **10**.
8. Mullen,J.R., Kaliraman,V., Ibrahim,S.S. and Brill,S.J. (2001) Requirement for three novel protein complexes in the absence of the sgs1 DNA helicase in *Saccharomyces cerevisiae*. *Genetics*, **157**, 103–118.
9. Fabre,F., Chan,A., Heyer,W.D. and Gangloff,S. (2002) Alternate pathways involving Sgs1/Top3, Mus81/Mms4, and Srs2 prevent formation of toxic recombination intermediates from single-stranded gaps created by DNA replication. *Proc. Natl. Acad. Sci. U.S.A.*, **99**, 16887–16892.
10. Bastin-Shanower,S.A., Fricke,W.M., Mullen,J.R. and Brill,S.J. (2003) The mechanism of Mus81-Mms4 cleavage site selection distinguishes it from the homologous endonuclease Rad1-Rad10. *Mol. Cell. Biol.*, **23**, 3487–3496.
11. Ho,C.K., Mazón,G., Lam,A.F. and Symington,L.S. (2010) Mus81 and Yen1 promote reciprocal exchange during mitotic recombination to maintain genome integrity in budding yeast. *Mol. Cell*, **40**, 988–1000.
12. Zakharyevich,K., Tang,S.M., Ma,Y.M. and Hunter,N. (2012) Delineation of joint molecule resolution pathways in meiosis identifies a crossover-specific resolvase. *Cell*, **149**, 334–347.
13. Ii,M. and Brill,S.J. (2005) Roles of SGS1, MUS81, and RAD51 in the repair of lagging-strand replication defects in Saccharomyces cerevisiae. *Curr. Genet.*, **48**, 213–225.
14. Hanada,K., Budzowska,M., Davies,S.L., van Drunen,E., Onizawa,H., Beverloo,H.B., Maas,A., Essers,J., Hickson,I.D. and Kanaar,R. (2007) The structure-specific endonuclease Mus81 contributes to replication restart by generating double-strand DNA breaks. *Nat. Struct. Mol. Biol.*, **14**, 1096–1104.
15. Froget,B., Blaisonneau,J., Lambert,S. and Baldacci,G. (2008) Cleavage of stalled forks by fission yeast Mus81/Eme1 in absence of DNA replication checkpoint. *Mol. Biol. Cell*, **19**, 445–456.
16. Shimura,T., Torres,M.J., Martin,M.M., Rao,V.A., Pommier,Y., Katsura,M., Miyagawa,K. and Aladjerm,M.I. (2008) Bloom's syndrome helicase and Mus81 are required to induce transient double-strand DNA breaks in response to DNA replication stress. *J. Mol. Biol.*, **375**, 1152–1164.
17. Errico,A. and Costanzo,V. (2012) Mechanisms of replication fork protection: a safeguard for genome stability. *Crit. Rev. Biochem. Mol. Biol.*, **47**, 222–235.
18. Petermann,E., Orta,M.L., Issaeva,N., Schultz,N. and Helleday,T. (2010) Hydroxyurea-stalled replication forks become progressively inactivated and require two different RAD51-mediated pathways for restart and repair. *Mol. Cell*, **37**, 492–502.
19. Regairaz,M., Zhang,Y.W., Fu,H.Q., Agama,K.K., Tata,N., Agrawal,S., Aladjem,M.I. and Pommier,Y. (2011) Mus81-mediated DNA cleavage resolves replication forks stalled by topoisomerase I-DNA complexes. *J. Cell Biol.*, **195**, 739–749.
20. Matos,J., Blanco,M.G., Maslen,S., Skehel,J.M. and West,S.C. (2011) Regulatory control of the resolution of DNA recombination intermediates during meiosis and mitosis. *Cell*, **147**, 158–172.
21. Gallo-Fernandez,M., Saugar,I., Ortiz-Bazan,M.A., Vazquez,M.V. and Tercero,J.A. (2012) Cell cycle-dependent regulation of the nuclease activity of Mus81-Eme1/Mms4. *Nucleic Acids Res.*, **40**, 8325–8335.
22. Schwartz,E.K., Wright,W.D., Ehmsen,K.T., Evans,J.E., Stahlberg,H. and Heyer,W.D. (2012) Mus81-Mms4 functions as a single heterodimer to cleave nicked intermediates in recombinational DNA repair. *Mol. Cell. Biol.*, **32**, 3065–3080.
23. Szakal,B. and Branzei,D. (2013) Premature Cdk1/Cdc5/Mus81 pathway activation induces aberrant replication and deleterious crossover. *EMBO J.*, **32**, 1155–1167.
24. Schwartz,E.K. and Heyer,W.D. (2011) Processing of joint molecule intermediates by structure-selective endonucleases during homologous recombination in eukaryotes. *Chromosoma*, **120**, 109–127.
25. Hollingsworth,N.M. and Brill,S.J. (2004) The Mus81 solution to resolution: generating meiotic crossovers without Holliday junctions. *Genes Dev.*, **18**, 117–125.
26. Whitby,M.C. (2005) Making crossovers during meiosis. *Biochem. Soc. Trans.*, **33**, 1451–1455.
27. Ciccia,A., McDonald,N. and West,S.C. (2008) Structural and functional relationships of the XPF/MUS81 family of proteins. *Annu. Rev. Biochem.*, **77**, 259–287.
28. Dehe,P.M., Coulon,S., Scaglione,S., Shanahan,P., Takedachi,A., Wohlschlegel,J.A., Yates,J.R., Llorente,B., Russell,P. and Gaillard,P.H.L. (2013) Regulation of Mus81-Eme1 Holliday junction resolvase in response to DNA damage. *Nature Struct. Mol. Biol.*, **20**, 598–603.
29. Cromie,G.A., Hyppa,R.W., Taylor,A.F., Zakharyevich,K., Hunter,N. and Smith,G.R. (2006) Single Holliday junctions are intermediates of meiotic recombination. *Cell*, **127**, 1167–1178.
30. Gaskell,L.J., Osman,F., Gilbert,R.J. and Whitby,M.C. (2007) Mus81 cleavage of Holliday junctions: a failsafe for processing meiotic recombination intermediates? *EMBO J.*, **26**, 1891–1901.
31. Tay,Y.D. and Wu,L. (2010) Overlapping roles for Yen1 and Mus81 in cellular Holliday junction processing. *J. Biol. Chem.*, **285**, 11427–11432.

32. Hunter,N. (2007) Meiotic recombination. In: Aguilera,A and Rothstein,R (eds). *Homologous Recombination*. Springer, Berlin, pp. 381–441.
33. Ehmsen,K.T. and Heyer,W.D. (2008) *Saccharomyces cerevisiae* Mus81-Mms4 is a catalytic structure-selective endonuclease. *Nucleic Acids Res.*, **36**, 2182–2195.
34. Fekairi,S., Scaglione,S., Chahwan,C., Taylor,E.R., Tissier,A., Coulon,S., Dong,M.Q., Ruse,C., Yates,J.R.,, Russell,P. *et al.* (2009) Human SLX4 Is a Holliday junction resolvase subunit that binds multiple DNA repair/recombination endonucleases. *Cell*, **138**, 78–89.
35. Munoz,I.M., Hain,K., Declais,A.C., Gardiner,M., Toh,G.W., Sanchez-Pulido,L., Heuckmann,J.M., Toth,R., Macartney,T., Eppink,B. *et al.* (2009) Coordination of structure-specific nucleases by human SLX4/BTBD12 is required for DNA repair. *Mol. Cell*, **35**, 116–127.
36. Svendsen,J.M., Smogorzewska,A., Sowa,M.E., O'Connell,B.C., Gygi,S.P., Elledge,S.J. and Harper,J.W. (2009) Mammalian BTBD12/SLX4 assembles a Holliday junction resolvase and is required for DNA repair. *Cell*, **138**, 63–77.
37. Castor,D., Nair,N., Declais,A.C., Lachaud,C., Toth,R., Macartney,T.J., Lilley,D.M., Arthur,J.S. and Rouse,J. (2013) Cooperative control of holliday junction resolution and DNA repair by the SLX1 and MUS81-EME1 nucleases. *Mol. Cell*, **52**, 221–233.
38. Wyatt,H.D., Sarbajna,S., Matos,J. and West,S.C. (2013) Coordinated actions of SLX1-SLX4 and MUS81-EME1 for Holliday junction resolution in human cells. *Mol. Cell*, **52**, 234–247.
39. Garner,E., Kim,Y., Lach,F.P., Kottemann,M.C. and Smogorzewska,A. (2013) Human GEN1 and the SLX4-associated nucleases MUS81 and SLX1 are essential for the resolution of replication-induced Holliday junctions. *Cell Rep.*, **5**, 207–215.
40. Ehmsen,K.T. and Heyer,W.D. (2009) A junction branch point adjacent to a DNA backbone nick directs substrate cleavage by *Saccharomyces cerevisiae* Mus81-Mms4. *Nucleic Acids Res.*, **37**, 2026–2036.
41. Fricke,W.M., Bastin-Shanower,S.A. and Brill,S.J. (2005) Substrate specificity of the *Saccharomyces cerevisiae* Mus81-Mms4 endonuclease. *DNA Repair*, **4**, 243–251.
42. Hutton,R.D., Craggs,T.D., White,M.F. and Penedo,J.C. (2010) PCNA and XPF cooperate to distort DNA substrates. *Nucleic Acids Res.*, **38**, 1664–1675.
43. Chapados,B.R., Hosfield,D.J., Han,S., Qiu,J.Z., Yelent,B., Shen,B.H. and Tainer,J.A. (2004) Structural basis for FEN-1 substrate specificity and PCNA-mediated activation in DNA replication and repair. *Cell*, **116**, 39–50.
44. Tsutakawa,S.E., Classen,S., Chapados,B.R., Arvai,A.S., Finger,L.D., Guenther,G., Tomlinson,C.G., Thompson,P., Sarker,A.H., Shen,B. *et al.* (2011) Human flap endonuclease structures, DNA double-base flipping, and a unified understanding of the FEN1 superfamily. *Cell*, **145**, 198–211.
45. Orans,J., McSweeney,E.A., Iyer,R.R., Hast,M.A., Hellinga,H.W., Modrich,P. and Beese,L.S. (2011) Structures of human exonuclease 1 DNA complexes suggest a unified mechanism for nuclease family. *Cell*, **145**, 212–223.
46. Chang,J.H., Kim,J.J., Choi,J.M., Lee,J.H. and Cho,Y. (2008) Crystal structure of the Mus81-Eme1 complex. *Genes Dev.*, **22**, 1093–1106.
47. Wright,W.D., Ehmsen,K.T. and Heyer,W.D. (2011) Assays for structure-selective DNA endonucleases. *Meth. Mol. Biol.*, **745**, 345–362.
48. Clegg,R.M. (1995) Fluorescence resonance energy transfer. *Curr. Opin. Biotechnol.*, **6**, 103–110.
49. Murchie,A.I., Clegg,R.M., von Kitzing,E., Duckett,D.R., Diekmann,S. and Lilley,D.M. (1989) Fluorescence energy transfer shows that the four-way DNA junction is a right-handed cross of antiparallel molecules. *Nature*, **341**, 763–766.
50. Lilley,D.M.J. and Clegg,R.M. (1993) The structure of the 4-way junction in DNA. *Annu. Rev. Biophys. Biomol. Struct.*, **22**, 299–328.
51. Wang,H., Yang,Y.G., Schofield,M.J., Du,C.H., Fridman,Y., Lee,S.D., Larson,E.D., Drummond,J.T., Alani,E.,, Hsieh,P. *et al.* (2003) DNA bending and unbending by MutS govern mismatch recognition and specificity. *Proc. Natl. Acad. Sci. U.S.A.*, **100**, 14822–14827.
52. Bustamante,C., Marko,J.F., Siggia,E.D. and Smith,S. (1994) Entropic elasticity of lambda-phage DNA. *Science*, **265**, 1599–1600.
53. Mazina,O.M., Rossi,M.J., Thomaa,N.H. and Mazin,A.V. (2007) Interactions of human Rad54 protein with branched DNA molecules. *J. Biol. Chem.*, **282**, 21068–21080.
54. Vance,J.R. and Wilson,T.E. (2002) Yeast Tdp1 and Rad1-Rad10 function as redundant pathways for repairing Top1 replicative damage. *Proc. Natl. Acad. Sci. U.S.A.*, **99**, 13669–13674.
55. Newman,M., Murray-Rust,J., Lally,J., Rudolf,J., Fadden,A., Knowles,P.P., White,M.F. and McDonald,N.Q. (2005) Structure of an XPF endonuclease with and without DNA suggests a model for substrate recognition. *EMBO J.*, **24**, 895–905.
56. Williams,R.S. and Kunkel,T.A. (2011) FEN nucleases: bind, bend, fray, cut. *Cell*, **145**, 171–172.
57. Dong,K.Z. and Berger,J. (2007) Structural basis for gate-DNA recognition and bending by typeIIA topoisomerases. *Nature*, **450**, 1201–1205.